Transactions on Engineering Sciences vol 13, © 1996 WIT Press, www.witpress.com, ISSN 1743-3533

Damage mechanics of steel components using micromechanics and structural dynamics models

H. Martikka
Department of Mechanical Engineering, Lappeenranta University of Technology, P.O. Box 20, FI 53851, Lappeenranta, Finland

Abstract

The damage mechanics of steels is studied using experimental and theoretical methods. Tensile tests and other tests are performed on a low alloy steel with varied grain sizes. Experimental results are analyzed using computer programs to obtain true stress-true strain curves. These results are simulated using microstructural dislocation dynamics models and theories on grain boundary, solution and dispersion hardening of multiphase and dispersion hardened alloyed materials. Using these models the initial discontinuous yielding and subsequent work hardening is satisfactorily predicted. Temperature and strain rate effects are also included. The applicability of FEM based Gurson-Tvergaard structural damage models are tested in estimating localised necking and fracture of the tensile tests. Mechanics of microstructural damage is visualized with a 2-D multibody dynamics simulation program.

1 Introduction

Damage mechanics approach of assessing deterioration of load carrying capacity of solid structures is based on void growth. The conventional microstructural and elastic-plastic models do not consider voids. But observations show that at fracture a ductile material becomes a porous solid. Over the years micromechanical void containing elastic-plastic yield models have been derived by Gurson [1], Tvergaard [2] and others. Zhang [3] tested these with examples and proposed new developments. There is a need for an integrated theory to predict the macroscopic behaviour by micromechanical models with minimal number of ambiguous parameters. The fracture mechanics approach assumes some distribution of initial cracks and their growth laws and

damage mechanics assumes some distribution of initial voids and their growth and coalescence laws.

The first goal in this study is to simulate the microstructural yielding and work hardening behaviour of a low alloy ferrite pearlite steel using micromechanical and dislocation mechanical models and to compare the results with tensile test experiments as by Martikka & al. [4]. Karlsson and Linden [5] have studied the plastic yielding and work hardening of ferrite pearlite structures using FEM and linear work hardening models with no voids. Mechanics of yielding and strengthening are reviewed by Ashby [6] and Martin [7]. The yield-point phenomena of carbon steel are discussed by Obataya and Kohno [8] using a random barriers theory. The upper and lower yield points and yield point elongation could be described systematically with the area fraction of pearlite in a ferrite matrix. The nonuniform yielding of mild steel plates was studied by Itoh & al. [9] and Gotoh [10] using dislocation mechanics models and FEM.

The second goal of the present study is to test the practical applicability of the G-T damage models of MARC [11] FEM program.The third goal is to simulate the damage mechanics in a qualitative way using a two-dimensional multibody and physical systems simulation program Working Model [12].

2 Experimental tests

Tensile and other tests were performed on a low alloy steel with varied grain sizes and analyzed to obtain true stress- true strain curves, Fig.1.

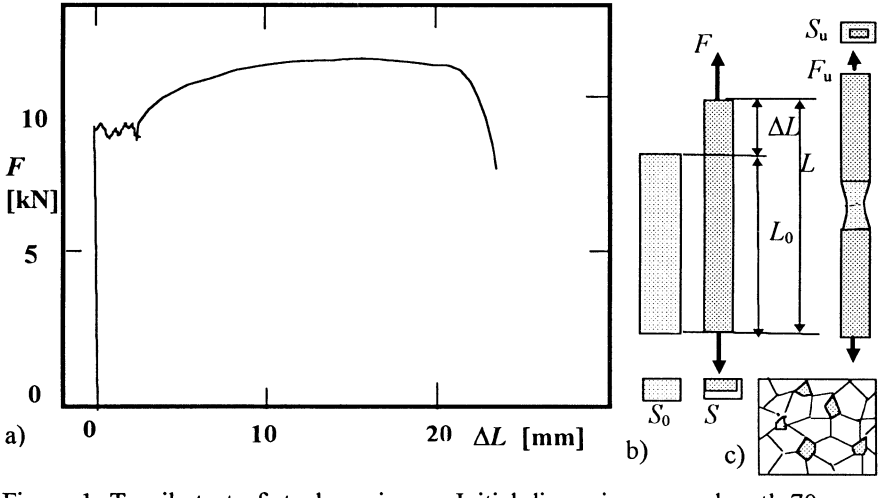

Figure 1: Tensile test of steel specimens. Initial dimensions were length 70 mm, thickness 2.6 and width 10 mm. a) Tensile test curve for series B/spec.3, b) schematic of the tensile test definitions, L_o, L are initial and current length, S_o,S_u are initial and fracture cross-sectional areas, c) schematic of the microstructure of ferrite and 0.17 (series B/6.) volume fraction of pearlite.

2.1 Metallography

The material was commercial low carbon steel of type Fe 37B SFS 200 with composition (in wt%) 0.13 C, 0.20 Si, 0.51 Mn, 0.017 P, 0.028 S, 0.15 Cr, 0.19 Ni supplied as hot rolled plates of 3 mm thickness.The present specimen (Ser.B/3) was heat treated at 750 °C/1h to grain size 0.012...0.011 mm.

2.2 Tensile tests

Analyzed tensile test curves of a specimen (ser.B/spec.3) are shown in Fig.2. The Bridgman correction was $B = (1+2/z)\ln(1+z/2)$ where $z = 0.75\varepsilon_u^{0.783}$ and $\varepsilon_u = \ln(1/(1-Z))$, $Z = 1 - S_u / S_0$ is reduction in area .The true stress is $\sigma_t = F_u / S_u$ and the axial tensile component at the neck is $\sigma_B = \sigma_t / B$, [13].

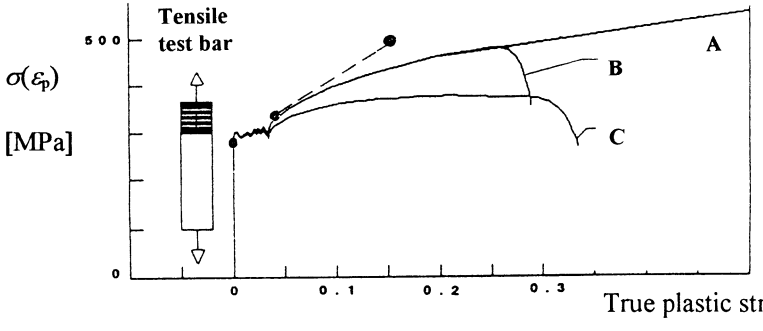

Figure 2: Conversion of tensile test curve for series B/spec.3. Curve C shows nominal stress F/S_o -linear strain $\varepsilon_n = \Delta L / L_0$. Curve B is true stress F/S -true strain $\varepsilon_p = \ln(1+\varepsilon_n)$. Curve A shows application of Bridgman correction to curve B, [4]. The two points were obtained by applying the G-T damage model of MARC FEM [11] to the curve A.

3 Theory of simulations

3.1 The yield stress of two ductile phases

It is assumed that both phases undergo the same strain, so the stresses will be different and the yield stress of the composite is given by the law of mixtures

$$\sigma_y = f_1\sigma_{y1} + (1-f_1)\sigma_{y2} \qquad (1)$$

where σ_{y1} and σ_{y2} are the yield stresses of the phases in isolation, and f_1 is the volume fraction of phase 1. In ferrite-pearlite structures pearlite is found to have only a small effect on the yield stress. Gladman & al [14] propose a modified formula with exponent $p = 0.01$ applied to volume fractions

$$\sigma_y = f_1^p\sigma_{y1} + (1-f_1^p)\sigma_{y2} \qquad (2)$$

3.2 The yield strength of ferrite

A general formula for the yield strength is

$$\sigma_y = \sigma_{Lud} + \Delta\sigma_G + \Delta\sigma_M + \Delta\sigma_T + \Delta\sigma_{KG} \tag{3}$$

3.2.1 Intrinsic strength

It is assumed that the intrinsic strength of pure polycrystalline material with some mobile dislocations may be combined to the Luders stress which corresponds to the discontinuous yielding and subsequent continuous yielding

$$\sigma_{Lud} = K \tag{4}$$

3.2.2 Solute hardening

When solute atoms pin dislocations they increase the strength by

$$\Delta\sigma_M = \alpha G c^{\frac{1}{2}} \tag{5}$$

where c is atomic fraction and α is a constant and G is shear modulus.
Assuming a linearly additive contribution of various sources of strength the solute hardening may be associated to the stress $\Delta\sigma_i$ [13]

$$\Delta\sigma_M = \Delta\sigma_i = 37\,(wt\%\mathrm{Mn}) + 83\,(wt\%\mathrm{Si}) + 2918\,(wt\%\mathit{free}\mathrm{N}) \tag{6}$$

3.2.3 Dislocation hardening

Increase of dislocation density hinders motion of dislocations and leads to increase of yield strength by an amount

$$\Delta\sigma_V = \beta G b \rho^{1/2} \tag{7}$$

where ρ is dislocation density and β is a constant, b is the Burgers vector. Dislocations are classified as geometrically necessary and statistically stored [6].

3.2.4 Particle hardening In a two-phase alloy deformation gradients cause geometrically necessary dislocations to be stored close to particles. Increment of hardening caused by particles is described by Ashby [6] as

$$\Delta\sigma_T = C_1 G\left[\frac{b f_p \varepsilon_p}{d}\right]^{1/2} \qquad C_1 = C_2 M^{3/2} \qquad C_2 = 0.25 \qquad M = 2 \tag{8}$$

where d is average particle diameter, ε_p is plastic strain, f_p is volume fraction of hard equiaxed particles in a ductile matrix with b and G constants, C_1 is a constant [6]. Here M is the orientation factor for bcc crystals . It is used to transform single crystal shear stress τ vs. shear strain γ relation $\tau(\gamma)$ into polycrystal $\sigma(\varepsilon)$ relation by

$$\tau = \sigma / M \quad , \quad \gamma = M\varepsilon \tag{9}$$

3.2.5 Grain boundary strengthening

If grain boundaries are regarded as obstacles to slip acting with slip distance equal to grain size D then the increment of yield strength due to grain boundaries and due to plastic strain ε_p is described by Ashby [6] as

$$\Delta\sigma_{KG} = C_4 G\left[\frac{b\varepsilon_p}{D}\right]^{1/2} \qquad C_4 = C_3 M^{3/2} \qquad C_3 = 0.35 \qquad M = 2 \qquad (10)$$

3.2.6 Grain size effect on yield hardening

The effect of polygonal grain size D (mm) on yielding is described by a Hall-Petch type equation with a coefficient $k_y = 22$ (MPa mm$^{1/2}$)

$$\Delta\sigma_G = k_y D^{-1/2} \qquad (11)$$

3.3 Transition from elastic to plastic yielding

The onset of plastic yielding is described by the dynamical theory of discontinuous yielding. This type of yielding is prominent in low alloy carbon steels. Three prerequirements for the occurrence of this type of yielding are proposed by Wyatt et al .[13]:

1. The first requirement is a low enough number of mobile dislocations. In bcc metals the in-grown dislocations ($10^4 \ldots 10^6$ disl/mm^2) are immobilized to give about 1 disl/mm^2 initially [6].
2. The second requirement is that the dislocation velocity increases with stress

$$v = \left[\frac{\sigma}{\sigma_0}\right]^n \qquad (12)$$

where σ is the applied stress and σ_0 is the stress for unit velocity. It is taken as $\sigma_0 = 180$ MPa for $v = 1$ mm/s and for iron $n = 35$ is used [13]. As the number of dislocations increases a linear work hardening law is assumed :

$$\Delta\sigma = q\varepsilon_p \qquad (13)$$

Wyatt et al. [13] estimate $q = 3000 \ldots 4000$ MPa. In the Luders range the effective hardening rate is smaller. Hence the dislocation velocity is retarded as the back stress $\Delta\sigma$ decreases the effective stress moving the dislocations

$$v = \left[\frac{\sigma - q\varepsilon_p}{\sigma_0}\right]^n \qquad (14)$$

3. The third requirement is rapid dislocation multiplication, involving double cross slip of screw dislocations and trailing lines of edge dislocation dipoles, which break up into prismatic loops and subsequently generate further dislocations by the Frank-Read type mechanism. The number of active dislocations has been roughly approximated by [13] :

$$\rho = f_m \cdot \left(\rho_0 + C\varepsilon_p{}^e\right) \qquad (15)$$

where f_m is the proportion of dislocations which are mobile (typically 0.1), ε_p is the plastic strain, ρ_0 is the initial dislocation density (disl/mm^2).For decarbonized iron $C = 1.6\ 10^7$ and $e = 0.8$ and for 0.2 percent iron $C = 4.7\ 10^5$ and $e = 1.5$ [13] .Now values $C = 1\ 10^7$ and $e = 1$ are chosen. The imposed strain rate $d\varepsilon / dt = \dot{\varepsilon}$ produces the following plastic strain per time

$$\dot{\varepsilon} = 0.5\, b \rho v \tag{16}$$

where the factor 0.5 averages the various orientations of slip planes. When equations (17), (18) and (19) are combined then the stress strain curve at initial discontinuous yielding is obtained as: (17)

$$\sigma = \Delta\sigma + \sigma_{\mathrm{Lud}} \qquad \sigma = q\varepsilon_p + \sigma_0 \left[\frac{\dot{\varepsilon} \cdot Rane}{0.5 b v_0 f_m \cdot Ranv \cdot Rant \cdot \left(\rho_0 + C\varepsilon_p^{\,e}\right)} \right]^{1/n}$$

where *Rane* is a random factor having equal probability between 1±0.1 for changing strain rate, *Ranv* is a random factor changing dislocation velocity due to the statistical effect of obstacle distribution and *Rant* is a random factor used to apply thermal activation. It is based on the model for dislocation velocity

$$v = s\nu e^{-\frac{\Delta G}{kT}} \tag{18}$$

where ΔG is the change of Gibbs free energy, ν is the frequency of vibration of the dislocation line against the obstacle, s is the mean distance traveled by dislocation after thermal activation has helped it to dislodge from the obstacle, k is Boltzmann's constant and T is absolute temperature.

3.4 Results of simulations

Tensile test results were simulated using present microstructural models, Fig. 3

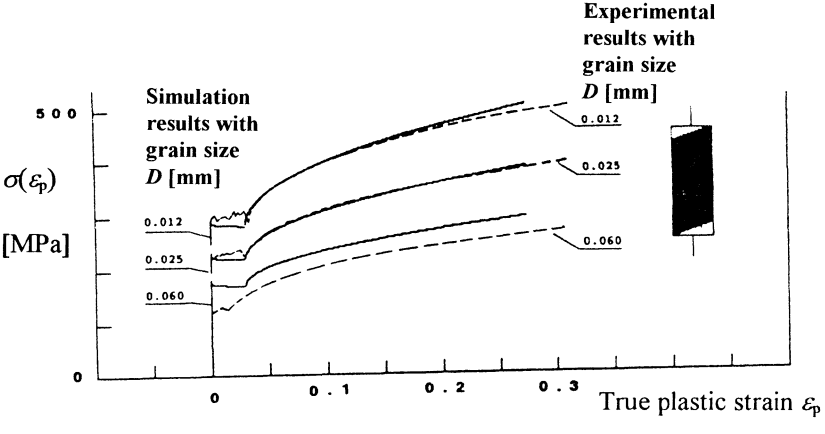

Figure 3: Comparison of true stress- true strain curves. Experimental curves and grain size D are B/3 with 0.012 mm, C/11 with 0.025 mm and D/16 with 0.06. Simulated curves are plotted with grain sizes D = 0.012, 0.025 and 0.06.

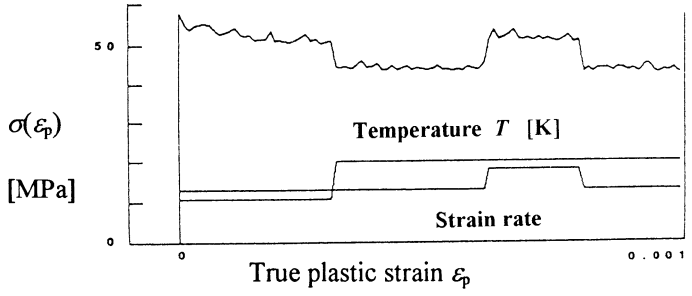

Figure 4: Simulation of true Luders stress - true strain tensile test showing initial discontinuous yielding. The effect of simulated changes of strain rate and temperature are also shown. Effective strain hardening rate was set to $q = 200$.

3.5 Necking initiation in tensile test

Necking is prerequisite for ductile fracture. Using a classical model the tensile force is the same through all cross-sections whose cross sectional area S is variable along axial direction x, $F = \sigma(x)S(x)$. At necking $dF = 0$ and the volume $V = SL$ is constant giving $dV = d(SL) = 0$ and $d\dot{S}/S = -\dot{\varepsilon}$.
Now the true stress -true strain model is in the continuous yielding parabolic

$$\sigma = \sigma_{\mathrm{Lud}} + K(\varepsilon - \varepsilon_{\mathrm{Lud}})^{\mathrm{m}} = 288 + 454(\varepsilon - 0.034)^{0.54} \qquad (19)$$

Now the strain rate sensitivity is $\delta = \partial \ln(\sigma) / \partial \ln(\dot{\varepsilon})$. But at room temperature $\delta = 0$ roughly. At the maximum force level $F = F_{\max}$, $dF = 0$

$$\frac{dS}{dx}(1 - m - \delta) = \frac{\delta}{\dot{\varepsilon}} \frac{d\dot{S}}{dx} \qquad (20)$$

The limit of stable strain with no necking is that if $dS > 0$ then for stability $d\dot{S} < 0$ whence $1 < m(\sigma - \sigma_{\mathrm{Lud}}) / ((\varepsilon - \varepsilon_{\mathrm{Lud}})\sigma) + \delta$ or now
$1 < 0.54\ (1 - 288/500)/(\varepsilon\text{-}0.034) + \delta$ whence $\varepsilon < 0.25$.
This is larger than the measured tensile test necking strain $\varepsilon_g = 0.2$

3.6 FEM damage model applications

3.6.1 Damage model theory

The modified Gurson model [1] for ductile metals is used. The yield criterion is used in the form [11] :

$$F = \left[\frac{\bar{\sigma}}{\sigma_{\mathrm{y}}}\right]^2 + 2q_1 f^* \cosh\left(\frac{q_2 \sigma_{\mathrm{kk}}}{2\sigma_{\mathrm{y}}}\right) - \left[1 + \left(q_1 f^*\right)^2\right] = 0 \qquad (21)$$

where $\bar{\sigma}$ is the von Mises equivalent stress and , $\sigma_{\mathrm{kk}} = \sigma_1 + \sigma_2 + \sigma_3 = 3\sigma_{\mathrm{m}}$ here the mean stress is the hydrostatic stress $\sigma_{\mathrm{h}} = \sigma_{\mathrm{m}}$, and σ_{y} is the flow stress of the matrix in current state.

3.6.2 Application results

Zhang [3] has studied damage using axially symmetric notched specimens (AX1) as shown in Fig.5. The load with diameter reduction is shown in Fig.5c.

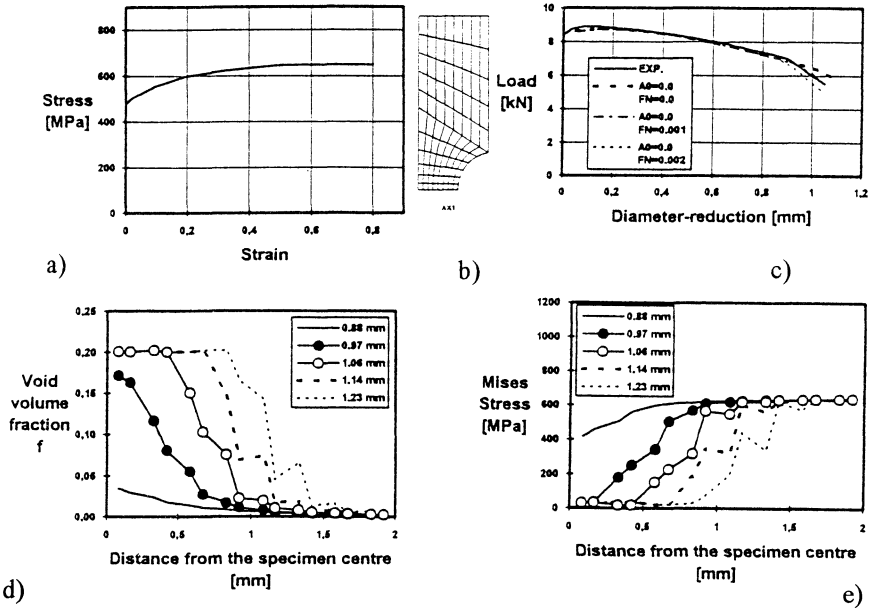

Figure 5: Results of Zhang [3]. Specimen : notched 1, minimum diameter = 4.0 mm, maximum diameter : 7.0 mm , notch radius = 1.75, Mesh AX1, material Fe510. a) Bridgman corrected true stress-true strain curve, b) notched specimen geometry, c) load-diameter reduction curves, exp = experimental, d) distribution of void volume fraction with various diameter reductions (mm), e) distribution of Mises equivalent stress in notched specimen No.1, with $f_f = 0.2$.

3.6.3 Present applications of FEM damage theory

3.6.3.1 Material properties The damage models of MARC FEM program [11] were applied to the tensile test results. One symmetric quarter was modelled. The goal was to simulate the fracture behaviour. The material is the same as the specimen Ser.B/3 [4], whose Bridgman corrected true stress-true strain tensile test curve is shown in Fig, 2, curve A. It was modelled linearly in the discontinuous and in the continuous regions.Young's modulus is $E = 210$ GPa. The Gurson damage model will be invoked using the strain controlled models. The parameters used are: First yield surface multiplier $q_1 = 1{,}5$, second yield surface multiplier $q_2 = 1{,}0$, initial void volume fraction $f_i = .005$, critical void volume fraction $f_c = .03$, failure void volume fraction $f_f = 0.15$, mean strain for nucleation 0.1, standard deviation .00408.

Inclusions contribute to the initial void volume fraction like the volume fraction of MnS inclusions. Its contribution can be estimated by the formula of Franklin as given by [3] $f_v = 0.054[S(\%) - 0.001/Mn(\%)]$. Now this gives f_v = 0.054(0.028 -0.001/0.51)= 0.0014.

3.6.3.2 Results The distribution of the void volume fraction and plastic strains are shown in Fig. 6. the models predict correctly fracturing at the middle.

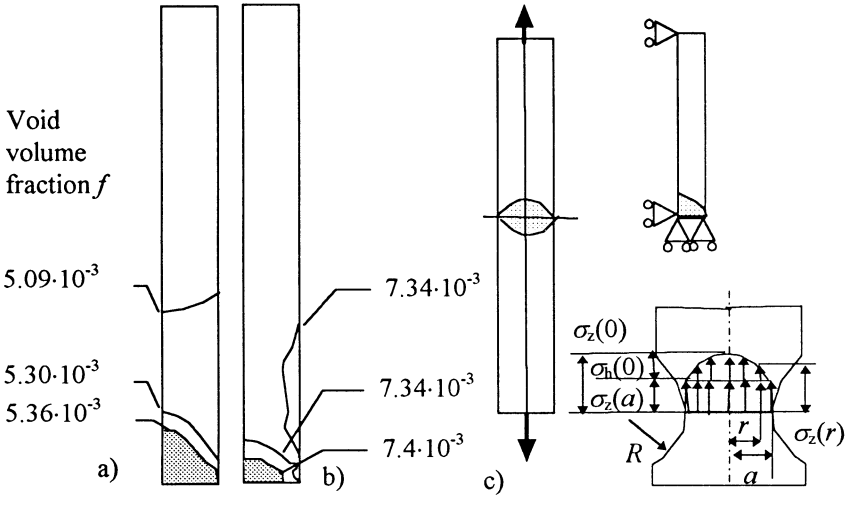

Figure 6: FEM [11] results of one quarter of the specimen serB/3, Fig.2. The true stress-true strain Bridgman corrected curve was used to calculate void volume fraction distribution f. a) Initial stage at plastic strain ε_p =.014, σ = 320 MPa, $f = 5.41\cdot10^{-3}..5.09\cdot10^{-3}$, b) Second stage at ε_p = .16, σ = 500 MPa , f = $7.26..7.43\cdot10^{-3}$, c) schematic models of the FEM model and necking area.

3.7 Tentative application of G-T model to tensile test analysis

From the true stress-true strain curves of Fig.2 it can be concluded that if no void nucleation and growth process would shappen then the stress would grow along the Bridgman correction line. A tentative and coarse idea is suggested from the tensile test curve analysis. Let us consider tensile test specimen where a is the radius of the neck cross section, R is the radius of curvature at the neck in the axial plane, Fig.6.At relative radius r/a the hydrostatic stress is $\sigma_h(r) = \sigma_z(a)g(r)$. Here $\sigma_z(a)$ is the uniform axial stress and $g(r)$ is function of radius r from centerline. The total axial stress at radius r is

$$\sigma_z(r) = \sigma_z(a) + \sigma_h(r) = \sigma_z(a)(g(r) + 1) \qquad (22)$$

The average value of the stress across the cross section is the true stress

$$\sigma_t = \overline{\sigma}_z(a) + \overline{\sigma}_h(r) = \sigma_z(a) + (B-1)\sigma_z(a) = B\sigma_z(a) \qquad (23)$$

The Bridgman corrected curve y_1 is a straight line, Fig. 2,curve A giving the true stress $y_1 = Y_n = \sigma_t$. The second curve y_2 is true stress without Bridgman correction *B*, Fig.2. The following tentative assumptions can be made

a The effective stress/yield strength $\bar{\sigma} / Y_n = y_2 / y_1$

b Hydrostatic stress /yield stress $\sigma_m / Y_n = (y_1 - y_2) / y_1$

This coarse estimate gives the mean value *f*. At each plastic strain step point the *f* value which satisfies the G-T equation [1,2] is calculated. The first $f = .0027$ and the final volume fraction was $f = 0.14...0.15$. Thus the maximum *f* can be about 0.2 which was obtained by Zhang [13] , Fig. (3) b.

3.8 Qualitative atomistic damage models

Damage simulation models can be made using Working Model [12], Fig.7. Atoms are modelled as planar disks which are attracted by a pairwise acting nonlinear forces or nonlinear springs. One available force type is (24)

$$F = -H \cdot self.mass \cdot other.mass / (\text{abs}(self.p - other.p))^h = -H \cdot m_i \cdot m_j / r_{ij}^h$$

where $h = 2$ or higher and H is a constant.The force interactions are calculated between all atom pairs m_i m_j depending on their radial distances r_{ij}. It can be seen that deformationa and fracture behaviour is qualitatively visualized. One possibility were to use difference of attractive and repulsive force terms depending on equilibrium distance r_o, actual distance r and exponents J and N as

$$F = C\left[\left(\frac{r_0}{r}\right)^J - \left(\frac{r_0}{r}\right)^N\right] \qquad (25)$$

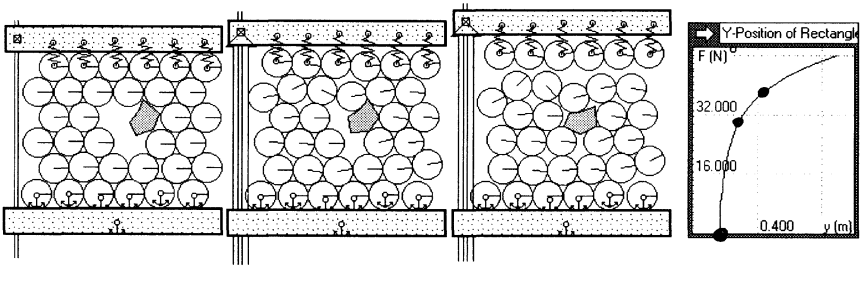

Figure 7: Tensile test simulation showing tensile force vs. displacement [12].

4 Conclusions

The following conclusions may be drawn:

- The tensile test of a basic low alloy steel can be satisfactorily simulated in the initial discontinuous and continuous work hardening range using microstructural dislocation dynamics models and theories on grain boundary,

solution and dispersion hardening of multiphase and dispersion hardened alloyed materials.

- The conventional models do not predict satisfactorily the basic process of necking and ductile fracture. Damage models offer realistic models but are still based on experimentally observed curves like tensile test curves.
- Damage models which are based on physical dislocation and atomistic models is promising but more development and simulation speed is needed.

Acknowledgements. The assistance in MARC FEM calculations of Mr. Seppo Toivanen,MSc,Econocap Engineering, and Mr.Jouni Könönen, BSc, in WM modelling , are gratefully acknowledged

References

1. Gurson A L, *Plastic flow and fracture behaviour of ductile materials incor porating void nucleation*, Ph.D dissertation, Brown University, 1975.
2. Tvergaard V. Material failure by void growth to coalescence, *Advances in Appl. mech.*,eds.J.W.Hutchinson & T.U.Wu, 83-151,AcademicPress, 1990.
3. Zhang, Zhiliang, *A practical micro-mechanical model. based local approach methodology for the analysis of ductile fracture of welded T- joints*, PhD thesis, Lappeenranta University of Technology, 1994
4. Martikka H., Eskelinen H., Suoranta R., Computer aided measurement of steel and composite machine elements and simulation based on micro-and macromechanics, editor: E.Niemi, *Proceedings of the 4th Finnish Mechanics days*, June 5-6, 1991, Lappeenranta , Finland
5. Karlsson G., Linden G.,Plastic deformation of ferrite pearlite structures in steel. *Materials Science and Engineering*, 17 (1975), p. 209-219.
6. Ashby M.F., The deformation of plastically non-homogeneous alloys, in Kelly A., Nicholson R.B. (editors), *Strengthening methods of crystals*, Applied science publishers Ltd., London.
7. Martin J.W., *Worked examples in the strength of metals and alloys*, The Inst.of metallurgists, Oxford, 1983, p. 12-56.
8. Obataya, Y. & Kohno S., A description of the yield-point phenomenon of carbon steel based on the random barriers theory, *JSME International Journal* , Series 1, Vol.33, No.3, 1990.
9. Itoh M, Yoshida F., Yamashita Y., Ohmori M., FEM analysis of nonuni-form yielding processes in mild steel plates under stretching, *JSME International Journal*, Series 1, Vol. 35, No.1, 1992.
10. Gotoh, M., Improvements of J2- deformation theory and their applications to FEM analyses of large elastic-plastic deformation. *JSME International Journal*, Series 1, Vol.33, No.2, 1990.
11. MARC Analysis Research Corporation, Rev.K.6, 1994.
12. Working Model, for Windows, Version 2.0, Knowledge Revolution.
13. Wyatt O.H., Dew-Hughes, *Metals, Ceramics and Polymers*, Cambridge University Press, 1974.
14. Gladman T.,McIvor I.D., Pickering F.B., J.I.S.I.210,1972, p.916